Enhanced Resolution Chirped Pulse Interferometry

Madeleine Bérubé

University of Waterloo

December 2nd, 2024

This work is being submitted as a partial fulfillment of the requirements of PHYS 437A.

Abstract

The goal of this research project was to investigate the enhancement of chirped pulse interferometry's signal resolution. To achieve this, a mathematical model of a chirped pulse interferometer was created in Mathematica. It was shown that applying a non-linear chirp to the pulses produces a final resolution comparable to that of the analogous quantum system, thus eliminating the remaining quantum advantage. Moreover, this report describes the impact of dispersion on the signal width for both conventional and non-linear chirped pulse interferometry. It was found that the non-linear method is insensitive to large amounts of dispersion. Finally, this research investigated the possibility of increasing the strength of the non-linear chirp to obtain even better resolution. The conclusion was that non-linear chirped pulse interferometry can have a resolution of at least 10% better than the quantum technique.

The first section of this report provides background information about the different types of interferometry compared in this project. This is followed by a description of the signal resolution, as well as the expected results for each type of interferometer. Next, the mathematical model is described, along with the process of obtaining the non-linear chirped pulses. Finally, the results are presented and discussed in section 3.

Contents

List of figures

List of tables

1 Introduction

This research project focuses on enhancing the resolution of an interferometry technique called chirped pulse interferometry (CPI). [1] The motivation for this project came from a disparity between classical and quantum interferometers: certain techniques have a better signal resolution than others. The goal of this project was to show that CPI, a classical technique, can produce a resolution comparable to that of the quantum technique. First, it is essential to understand the basics of interferometry and the different types of interferometers.

1.1 Interferometry techniques

When two or more waves overlap, they produce an interference pattern from the superposition of the individual crests and troughs of the waves. The interaction of waves in this manner is called interference, and the technique of extracting information from interference patterns is known as interferometry. One of the most important types of interferometry is the interference of electromagnetic waves (light).

The interference of light is principally used for metrology purposes, where it enables precise measurements. Some applications include measuring distances, electric fields, temperature, pressure, and surface topography. [2] To measure these quantities, several different interferometry techniques exist, each with its advantages and disadvantages. Three techniques are discussed in this report: white light interferometry and chirped pulse interferometry (CPI), which are classical techniques, and Hong-Ou-Mandel (HOM) interferometry, a quantum technique. [2][1][3]

1.1.1 Coherence time

These three techniques are all low-coherence interferometry systems, which means they can perform absolute measurements of a sample. The resolution of this measurement depends on the coherence time of the system. The coherence time can be described as the extent of time over which a light wave resembles a sinusoidal wave, such that its phase can be reliably predicted. [4] The coherence time of a pulse of light is proportional to the inverse of the frequency bandwidth of the pulse.

$$\tau_{coh} \sim \frac{1}{\Delta\omega}$$

Therefore, a broadband light source has a small coherence time, whereas a narrow-band source has a large coherence time. Ultimately, the quality of the measurement performed by the interferometer is dependent on the coherence time of the pulse: smaller coherence times lead to better resolution. The topic of signal resolution is discussed in more detail in section 1.2.

1.1.2 Dispersion cancellation

Interferometry is often used to precisely measure a sample, which is placed in the interferometer. When light passes through a sample, it undergoes dispersion. This comes from the fact that the speed of light inside a material is frequency-dependent. For example, red light travels faster than blue light in glass. [4] This causes light pulses to get stretched out in time when passing through a dispersive medium. In interferometry, dispersion is unfavourable because it increases the width of the signal, thus degrading the resolution of the measurement.

Quantum interferometers were the first systems to demonstrate dispersion cancellation, which means the output signal was insensitive to the effects of dispersion. [5] While dispersion cancellation was originally thought to be unique to systems with entangled photons, it has been shown that classical systems can also exhibit it. [6] One of these classical systems is chirped pulse interferometry, which will be discussed in section 1.1.5. Dispersion cancellation is a favourable effect in interferometry since it allows for measurements of samples without degrading the resolution.

1.1.3 White Light Interferometry

White light refers to visible light containing all wavelengths of the visible spectrum equally. Figure 1 contains a schematic drawing of a simple white light interferometer. The input light source, which is usually a laser, passes through a beamsplitter, which separates the light equally into two beams. Each beam travels down a different path, either the reference arm or the sample arm. The beam travelling in the reference arm gets delayed by some time, τ, by displacing a moveable mirror and changing the path length. Moving the mirror further or closer along the path increases or decreases the distance light must travel by $c\tau$, where c is the speed of light. In the sample arm, the beam travels a distance L into a sample material before reflecting. Both beams are ultimately recombined in the beamsplitter and then directed onto a detector. The detected interference pattern contains information about the path lengths travelled by the light.

Figure 1: A white light interferometer

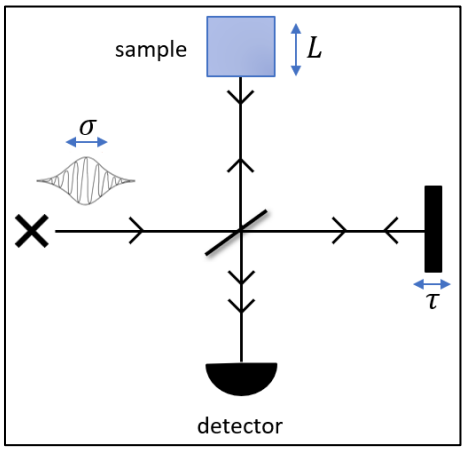

White light interferometers can measure an absolute time delay, which corresponds to an absolute position. Here is how this works: the time delay set with the moveable mirror is a known quantity in the system. When the pulses in each arm travel the same distance, the interference at the detector will be destructive. In this case, the time delay is equal to the length of time that the pulse travelled in the sample arm. Thus, by finding the time delay that creates this interference pattern, an absolute measurement of the sample can be made. One application of white light interferometry is optical coherence tomography (OCT). [7] OCT is a three-dimensional non-invasive medical imaging technique. Using white light interferometry, 3D scans of the interior of a sample can be reconstructed, without damaging or invading it. OCT is often used to image the retina and other eye parts, and it is currently a common and successful imaging method in ophthalmology. [7]

White light interferometry has the advantage of producing high-intensity signals, on the micro- to milli-watt scale. This increases detection abilities, which makes white light interferometry a popular choice for clinical applications. However, it will be seen in section 1.2 that there are disadvantages of using white light interferometry, due to its sensitivity to dispersion and its signal resolution.

1.1.4 Hong-Ou-Mandel Interferometry

The Hong-Ou-Mandel interferometer is a quantum technique that uses the interference of two pairs of entangled photons. [3] Figure 2 shows an example of a HOM interferometer. The pairs of entangled photons are produced via spontaneous parametric down-conversion (SPDC). The pairs then travel through a reference and sample arm, similar to the white light interferometer. If the photons arrive at the beamsplitter simultaneously (which means they spent equal time in each arm), they will interfere and be detected in coincidence in the two single-photon detectors at the end of the interferometer. By measuring detection coincidences at different time delays, the HOM interferometer provides an absolute measurement of the sample path length.

Figure 2: A HOM interferometer

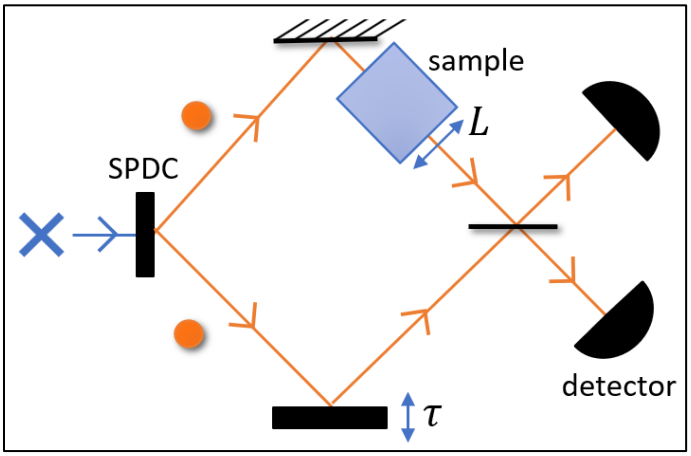

The HOM interferometry method has been used for optical coherence tomography, referred to as quantum optical coherence tomography (QOCT) [8][9][10]. While white light interferometry has high-powered signals, the quantum signal is orders of magnitude lower. HOM interferometers typically measure signals on the pico- to femto-watt scale, since they are ultimately detecting single photons. [11]. This presents challenges in detecting the signal. However, quantum interferometry presents advantages when it comes to dispersion cancellation, as mentioned in section 1.1.2, and signal resolution, which will be discussed in section 1.2.

1.1.5 Chirped Pulse Interferometry

Chirped pulse interferometry is a classical technique that has the combined advantage of white light interferometry's high-power output and HOM's dispersion cancellation. Instead of using a broadband white light source or pairs of entangled photons, CPI used chirped pulses. A chirped pulse is a pulse where the frequency changes with time, as illustrated in figure 3.

Figure 3: A chirped pulse

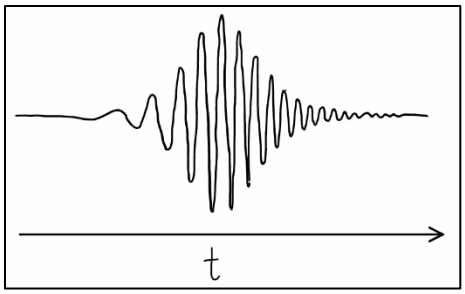

If the pulse in figure 3 is defined as a chirped pulse, then an anti-chirped pulse is one where the frequency decreases with time. In a chirped pulse interferometer, a combination of chirped and anti-chirped pulses travel through the reference and sample arms of the device. Then, the two pulses are combined in a non-linear material, where they undergo sum-frequency generation (SFG). SFG is a non-linear optics method that combines two pulses as the product of their intensities. [12] The combined pulse is then detected in the detector at the end of the interferometer. CPI can be thought of as a time-reversed, classical version of the HOM interferometer [1]. This system is presented in the diagram in figure 4.

Figure 4: A chirped pulse interferometer

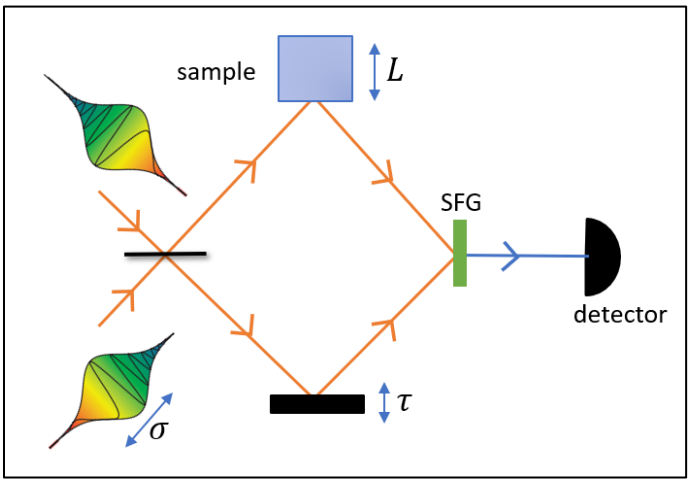

CPI has the advantage of a higher signal intensity than the quantum interferometer. Moreover, CPI exhibits dispersion cancellation, which makes it an improvement over white light interferometry. [1] However, while traditional CPI resolution is better than that of white light interferometry, it is worse than the resolution of HOM interferometry, the analogous quantum system.

1.2 Signal Resolution

As discussed in the three techniques above, the power output, sensitivity to dispersion, and signal resolution are factors that impact the quality of interferometry. This section will examine the signal resolution of interferometric systems, and compare the results for white light, HOM, and CPI.

The signal from a low-coherence interferometer has a characteristic dip shape, shown in figure 5. In this plot, the x-axis displays the time delay, set in the reference arm of the interferometer. The y-axis is the intensity of the signal. When the time that light takes to travel in the reference arm exactly matches the time that it takes in the sample arm, the intensity of the signal goes to zero. This is due to the interference of the pulses or the photons.

By scanning over a range of time delay values and measuring the output intensity, the dip shape can be obtained for the system. The resolution of the signal refers to the width of the dip, $\Delta\tau$. A better resolution has a narrower dip width since the true value of the time delay can be more precisely determined.

Figure 5: Signal dip from interferometry

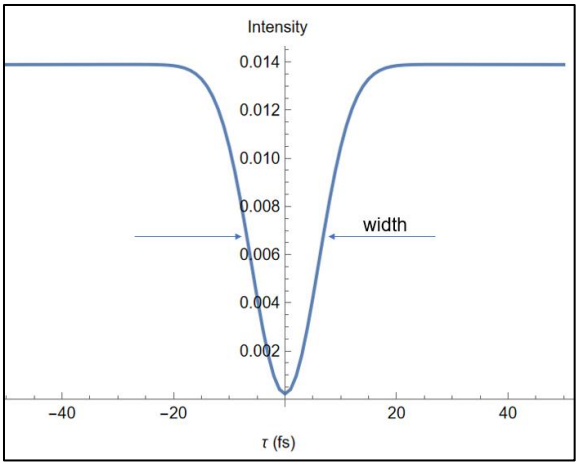

As mentioned in section 1.1, the coherence time of the pulses used in the interferometer impacts the resolution of the signal. A short coherence time leads to a narrower signal width. For white light interferometry, it might seem as though increasing the bandwidth, $\Delta\omega$, of the pulses will improve the resolution, since $\tau_{coh} \sim \frac{1}{\Delta\omega}$. However, a broader pulse in time will get more stretched out by dispersion, which ultimately has a negative impact on the signal width. In the absence of dispersive material, white light interferometers have a signal width that is twice the width of the original pulse:

$$\Delta\tau_{white} = \frac{2}{\Delta\omega}$$

For the quantum technique, the signal width is simply equal to the original bandwidth of the photon. This is an improvement by a factor of two from white light interferometry.

$$\Delta\tau_{HOM} = \frac{1}{\Delta\omega}$$

Finally, the CPI signal width is proportional to $\sqrt{2}$ of the original pulse width.

$$\Delta\tau_{CPI} = \frac{\sqrt{2}}{\Delta\omega}$$

This factor of $\sqrt{2}$ is explained in section 2.3.

While CPI resolution is better than white light interferometry, the factor of 2 achievement of the HOM interferometer puts the quantum system at an advantage over both. This motivated the following question: can CPI, a classical system, achieve the same resolution as a quantum interferometer? The objective of this project was to show that the resolution of the signal from CPI is comparable, and potentially better, than that of the quantum system. This would eliminate any advantage retained by the quantum system and make dispersion-cancelled interferometry using CPI a convenient and suitable alternative.

2 Theoretical Approach

2.1 Mathematical model of CPI

To investigate the enhancement of the CPI resolution, a mathematical model of an interferometer was developed in Mathematica. The following sections describe the approach used to translate each part of the interferometer into code.

2.1.1 Input laser pulse

The original laser pulse is modelled by an electric field, represented in both the time and frequency domain, $E_{laser}(t)$ and $E_{laser}(\omega)$. For this project, Gaussian pulses were used, with a full-width half-maximum (FWHM) σ.

$$E_{laser}(t) = \exp\left[\frac{-2\ln 2}{\sigma^2}(t - t_0)^2\right]\exp[-i\omega_0 t]$$

The first term corresponds to the Gaussian pulse, and the second is the carrier frequency term, centering the pulse (in the frequency domain) at ω_o. The parameters in this model were chosen to replicate values that would be used in a real experiment. The carrier frequency was chosen to be 2355 THz, or 2.355 fs^{-1}, which corresponds to an 800 nm laser. The FWHM was set to 10 fs. The pulse is centered at 200 ps in the time domain, which was chosen to ensure that $E_{laser}(\omega)$ remained within the corresponding frequency range when Fourier transformed. Table 1 summarizes the values used in this mathematical model.

Table 1: Input parameters for calculations

Parameter	Value
Minimum value for time range, t_{min}	0 ps
Maximum value for time range, t_{max}	400 ps
Central time value, t_0	200 ps
Carrier frequency, ω_0	2.355 fs^{-1}
Number of points used in time domain calculations, N	$2^{16} = 65536$
Original pulse FWHM width, σ	10 fs

2.1.2 Chirped pulses

Pulse chirping is achieved by applying a phase, $\phi(\omega)$, to the original pulse. Experimentally, this is done using a device called a spatial light modulator (SLM), but mathematically, it corresponds to multiplying the electric field of the pulse by $e^{i\phi(\omega)}$. Applying a phase that is quadratic in frequency, such as

$$\phi_{\pm}(\omega) = \pm A_{lin}(\omega - \omega_0)^2$$

leads to a chirped pulse whose frequency changes linearly with time. For this reason, $\phi(\omega)$ will be referred to as a linear phase function, which provides linear chirp. The positive and negative functions correspond to chirped and anti-chirped pulses respectively. The factor A_{lin} changes the strength of the chirp (how stretched the pulses become). This parameter was chosen to increase the width of the pulse by a factor of 1000. To take the pulse from a width of 10 fs to 10 000 fs, the required value for A_{lin} was 1300 fs^2.

The chirp must be applied to the pulses in the frequency domain, so the Mathematica function for discrete Fourier transforms was first applied to the laser pulse.

$$E_{laser}(\omega) = \text{Fourier}[E_{laser}(t)]$$

The chirped and anti-chirped pulses are given by

$$E_C(\omega) = E_{laser}(\omega)\exp[i\,\phi_+(\omega)] = E_{laser}(\omega)\exp[iA_{lin}(\omega - \omega_0)^2]$$

$$E_A(\omega) = E_{laser}(\omega)\exp[i\,\phi_-(\omega)] = E_{laser}(\omega)\exp[-iA_{lin}(\omega - \omega_0)^2]$$

2.1.3 Beamsplitter

Next, the pulses get combined in the beam splitter, such that a combination of chirped and anti-chirped pulses travel through each arm of the interferometer. This is represented by the sum of the electric fields of the pulses.

$$E_{reference}(\omega) = E_C(\omega) + E_A(\omega)$$

$$E_{sample}(\omega) = E_C(\omega) - E_A(\omega)$$

The negative sign in the 2nd equation comes from the fact that the transformation must be unitary and energy must be conserved.

2.1.4 Time delay in the reference arm

Within their respective arms, the pulses acquire either a time delay or dispersion. The time delay is represented by a linear phase of $e^{i\omega\tau}$, which results in the following pulse.

$$E_{reference}(\omega, \tau) = [E_C(\omega) + E_A(\omega)]\exp[i\omega\tau]$$

2.1.5 Dispersion in the sample arm

The dispersion is added to the sample beam by a quadratic phase. This phase is related to the sample material's wavevector, $k(\omega)$ and well as the length of the sample in the interferometer arm, L. The corresponding equation is given by:

$$\phi_{disp}(\omega) = k(\omega)L$$

Where the wavevector is:

$$k(\omega) = \frac{\omega\, n(\omega)}{c}$$

In this equation, c is the speed of light and $n(\omega)$ is the index of refraction of the sample material.

The wavevector can be Taylor-expanded around the central frequency carrier, ω_0.

$$k(\omega) = \left[k(\omega_0) + \frac{dk}{d\omega}\bigg|_{\omega_0}(\omega - \omega_0) + \frac{1}{2}\frac{d^2k}{d\omega^2}\bigg|_{\omega_0}(\omega - \omega_0)^2 + \cdots\right]$$

In this model, the first two terms are neglected, since the first term simply adds a constant phase, and the 2nd term adds a constant time delay. The interesting phenomenon is the term with quadratic frequency dependence, which stretches out the pulse in the time domain.

$$\phi_{disp}(\omega) = \left[\frac{1}{2}\frac{d^2k}{d\omega^2}\bigg|_{\omega_0}(\omega - \omega_0)^2\right]L$$

To simplify notation, the coefficient for the dispersion is represented by ϵ, such that the phase applied to the pulse in the sample arm is:

$$\phi_{disp}(\omega) = [\epsilon(\omega - \omega_0)^2], \qquad \epsilon = \frac{1}{2}\frac{d^2k}{d\omega^2}\bigg|_{\omega_0} L$$

And the corresponding pulse is:

$$E_{sample}(\omega, \epsilon) = [E_C(\omega) - E_A(\omega)]\exp[i\epsilon(\omega - \omega_0)^2]$$

To calculate the sample material's wavevector, the Sellmeier equation for index of refraction was used. [13] This is an empirical equation that relates the index of refraction to the wavelength.

$$n(\lambda) = \left[1 + \frac{B_1\lambda^2}{\lambda^2 - C_1} + \frac{B_2\lambda^2}{\lambda^2 - C_2} + \frac{B_3\lambda^2}{\lambda^2 - C_3}\right]^{\frac{1}{2}}$$

The coefficients B_i and $C_i, i = 1,2,3$, are experimentally determined. The Sellmeier equation was converted into a function of frequency, using the relationship between wavelength and frequency, $\lambda = \frac{2\pi c}{\omega}$.

$$n(\omega) = \left[1 + \frac{B_1\left(\frac{2\pi\omega}{c}\right)^2}{\left(\frac{2\pi\omega}{c}\right)^2 - C_1} + \frac{B_2\left(\frac{2\pi\omega}{c}\right)^2}{\left(\frac{2\pi\omega}{c}\right)^2 - C_2} + \frac{B_3\left(\frac{2\pi\omega}{c}\right)^2}{\left(\frac{2\pi\omega}{c}\right)^2 - C_3}\right]^{\frac{1}{2}}$$

From this, the wavevector for the material can be obtained by multiplying by a factor of $\frac{\omega}{c}$.

$$k(\omega) = \frac{\omega}{c}\left[1 + \frac{B_1\left(\frac{2\pi\omega}{c}\right)^2}{\left(\frac{2\pi\omega}{c}\right)^2 - C_1} + \frac{B_2\left(\frac{2\pi\omega}{c}\right)^2}{\left(\frac{2\pi\omega}{c}\right)^2 - C_2} + \frac{B_3\left(\frac{2\pi\omega}{c}\right)^2}{\left(\frac{2\pi\omega}{c}\right)^2 - C_3}\right]^{\frac{1}{2}}$$

In this model, the sample material selected was BK7 glass, which is a common type of glass used in laboratories. The values of B_i and C_i for BK7 have been determined and tabulated by previous experiments; the results are in table 2. [14]

Table 2: BK7 Sellmeier coefficients

Parameter	Value
B_1	1.03961212
B_2	0.231792344
B_3	1.01046945
C_1	$6.00069867 \times 10^{-3}\mu m^2$
C_2	$2.00179144 \times 10^{-2}\mu m^2$
C_3	$1.03560653 \times 10^{2}\mu m^2$

Using these values for the Sellmeier coefficients, the 2nd derivative of the wavevector was calculated in Mathematica, evaluated at the carrier frequency, ω_0, and multiplied by $\frac{1}{2}L$. This gave a value for the dispersion coefficient as a function of the amount of glass in the sample path.

$$\epsilon = 0.0223308\ L$$

Note that the amount of glass is a measure of the amount of dispersion in the system. More glass will lead to more dispersion.

Finally, the dispersion was applied to the field of the pulse in the sample arm.

$$E_{sample}(\omega, L) = [E_C(\omega) - E_A(\omega)] \exp[0.0223308\ i\ L\ (\omega - \omega_0)^2]$$

2.1.6 Sum-frequency generation and output intensity

At the end of the interferometer, the sample and reference beams are combined in a SFG process, which creates the interference pattern. In the time domain, the SFG signal is the product of the two fields. Mathematica's inverse Fourier function was used to convert the pulses from the frequency to the time domain. Then, they were multiplied together to get the SFG signal in time.

$$E_{SFG}(t, \tau, L) = E_{reference}(t, \tau)\ E_{sample}(t, L)$$

The detector at the end of the CPI interferometer detects the intensity of the light. To get the intensity of the SFG signal, it was Fourier transformed back to the frequency domain and squared.

$$I_{SFG}(\omega, \tau, L) = |E_{SFG}(\omega, \tau, L)|^2$$

This is the signal that would be measured by the detector at the end of the chirped pulse interferometer for a given value of time delay, τ, and dispersion, L.

2.1.7 Obtaining the dip

As described in section 1.2, a measurement with a low-coherence interferometer is obtained by scanning over a range of time delay values and measuring the output intensity. Finding the value of τ where the intensity goes to zero is the equivalent of measuring the distance light travelled in the sample arm, thus providing a measurement of the sample.

In this model, the time delay values ranged from -50 fs to 50 fs, in 1 fs intervals. Note that a negative time delay simply means that the reference beam path was shortened, instead of lengthened. The intensity was calculated at every time delay value over the entire range of frequency values and a color plot was created with the results. This plot contains the frequency values on the y-axis, time delay on the x-axis, and intensity plotted in colour for each value of τ and ω. Figure 6 shows the results for the model without dispersion.

Figure 6: The SFG intensity over a range of τ values

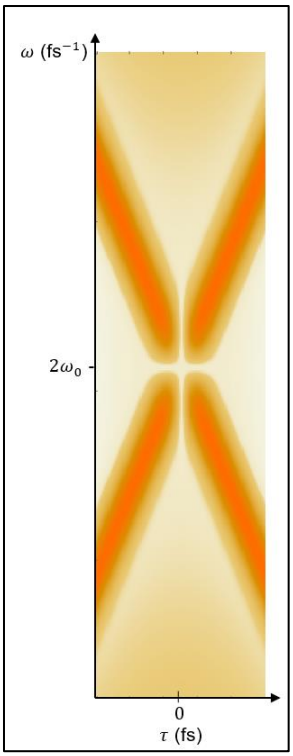

Finally, to obtain the dip, the sum of all the intensity values for each time delay was calculated. When plotting the summed intensity as a function of time delay, the signal dip is obtained. This is shown in figure 7.

Figure 7: Signal dip for linear CPI, no dispersion

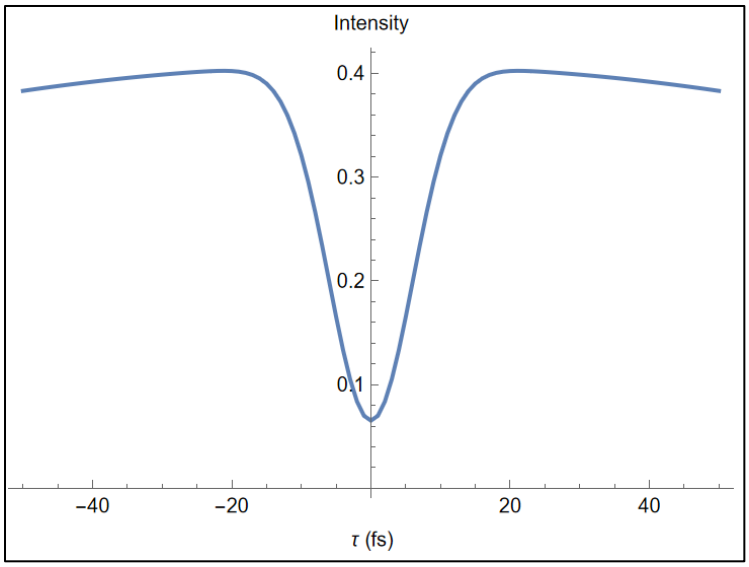

2.1.8 Resolution of the signal

The last step in quantifying the resolution of the signal is to fit the dip with a Gaussian function and extract the FWHM value. This was done through a chi-square minimization process. A Gaussian-shaped fitting function was created, with estimates for the initial parameters. The χ^2 values were calculated based on how well the function agreed with the dip, and Mathematica's FindMinimum function found the parameters that minimized χ^2. The FWHM of the dip is a measure of the resolution of the signal.

Note that for Gaussian-shaped pulses, the bandwidth is measured using the inverse of the FWHM of the pulse in time, σ. Therefore, we expect the resolution of the signal for CPI to be $\Delta\tau_{CPI} = \frac{\sqrt{2}}{\Delta\omega} = \sqrt{2}\sigma$.

2.2 Previous work

Before describing the enhancement of CPI, previous work on this topic must be acknowledged. This work is the continuation of the research performed by UWaterloo MSc graduate Michael Mazurek. [15] In his thesis, Mazurek showed that applying a non-linear phase function to the pulses resulted in a signal width equal to that of the quantum system.

$$\Delta\tau_{CPI,non-linear} = \sigma$$

Where σ is the FWHM width of the original pulse. This project furthers Mazurek's result by examining the impact of dispersion on non-linear CPI. While CPI is generally insensitive to dispersion, in the limit of large amounts of dispersive material, the signal width does begin to increase. This work compares the large dispersion limit for linear and non-linear CPI. Moreover, this project examines the further enhancement of the resolution by increasing the strength of the non-linear chirp, with the goal of achieving a better signal width than HOM interferometry.

2.3 Non-linear chirp

To enhance the resolution of the chirped pulse interferometer, it is crucial to first understand why the signal width scales with $\sqrt{2}$, instead of factors of 1 or 2, such as the quantum and white light systems. This has to do with the fact that the intensity of the SFG signal is proportional to the square of the combined electric fields. As seen in section 2.1.6, the chirped and anti-chirped pulses get combined non-linearly through SFG, and the measured intensity is the square of this electric field. Linearly chirped pulses have a Gaussian profile, and the square of two Gaussian intensity functions results in another Gaussian, with a width that is exactly $\sqrt{2}$ narrower in the frequency domain. Ultimately, this leads to the width being wider by $\sqrt{2}$ in the time domain.

This can be seen by examining the spectral content of the chirped pulse, drawn in figure 8 (left). The frequencies in the middle part of the pulse will contribute more to the final intensity than the frequencies on the sides, resulting in a final Gaussian that has a width $\sqrt{2}$ broader in time.

To improve CPI resolution, one solution is to find a phase function that causes the chirped pulse to have a constant-frequency intensity profile. Thus, when SFG is performed, all frequencies contribute equally to the signal, and there is no additional factor of $\sqrt{2}$. This type of chirped pulse resembles a top hat, as seen in figure 8 (right).

Figure 8: Intensity profiles for Gaussian (left) and top hat (right) pulses

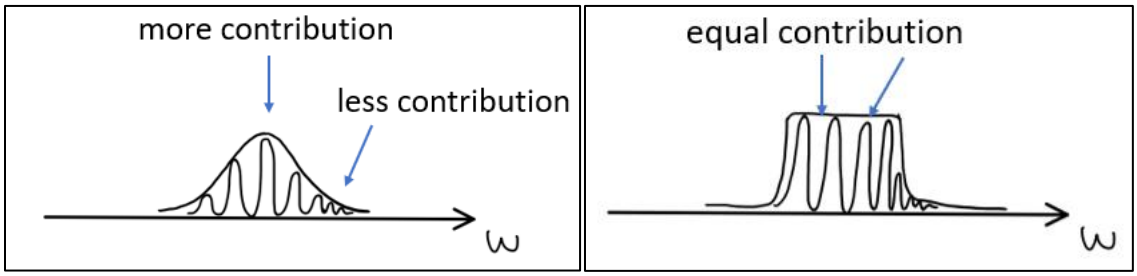

It was shown in Mazurek's thesis that a phase function which applies a non-linear chirp to the pulses gives rise to this top hat profile. [15] For this reason, this method of CPI will be referred to as non-linear CPI. The function that Mazurek developed for this purpose is proportional to the error function:

$$\phi_{\pm}(\omega) = \pm A_{erf}\left[\frac{e^{-x^2}-1}{\sqrt{\pi}} + x\,\mathrm{erf}(x)\right], \qquad x = \frac{2(\omega-\omega_0)\sigma}{\sqrt{2\log(256)}}$$

Here, A_{erf} sets the strength of the chirp, $\mathrm{erf}(x)$ is the error function, and σ is the FWHM of the original pulse. After applying this phase function to create chirped and anti-chirped pulses, the same procedure is followed as for the linear CPI model, described in section 2.1.

2.3.1 Comparison with linear CPI

The final step in creating this mathematical model of enhanced resolution CPI is to establish a method for comparing the linearly and non-linearly chirped pulses. In conventional CPI, the amount of chirp a pulse has received is defined by how much its width has increased. For example,

creating a chirped pulse with a FWHM of 10 ps, when the original pulse had a FWHM of 10 fs, corresponds to a chirp of 1000.

Since the non-linear chirped pulses do not have Gaussian profiles, their FWHM cannot be defined. To be able to compare them to the linear CPI, the width of the non-linear pulse was taken to be half the width of the rectangle of its intensity profile. Therefore, the two types of pulses receive the same amount of chirp if their widths line up when overlayed, such as in figure 9.

Figure 9: Intensity profiles for linear (red) and non-linear (blue) chirped pulses

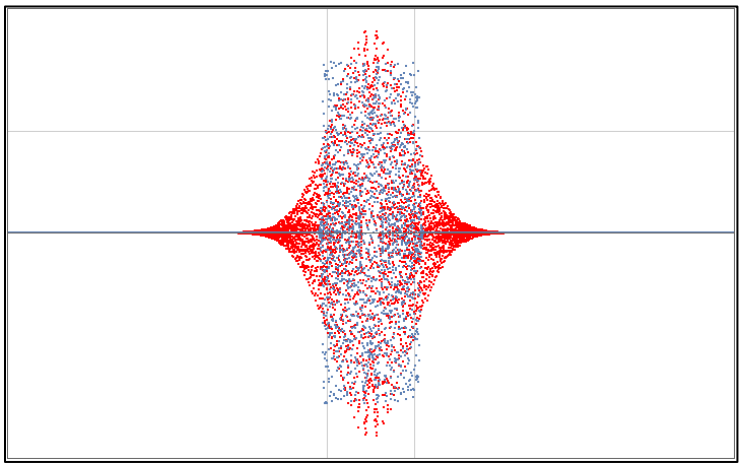

The vertical lines represent the FWHM of the linear (Gaussian-shaped) chirped pulse. For the scope of this project, the two widths were determined to be equal by visual inspection when plotted together. This corresponded to a value of $A_{erf} = 93\ \text{fs}^2$.

3 Results and Discussion

In all these calculations, an original pulse width of 10 fs was used, and the pulses were chirped to 10 ps (chirp factor of 1000).

3.1 Without dispersion

For the CPI model without dispersion, the resolution was found to be 14.1422 fs. This agrees with the expected result of

$$\Delta\tau_{CPI,linear} = \sqrt{2}\sigma$$

For the non-linear CPI model without dispersion, the resolution was found to be 10.043 fs. This is the same resolution that would have been obtained by an equivalent quantum interferometer. This result is also consistent with the relationship found by Mazurek. [15]

$$\Delta\tau_{CPI,non-linear} = \sigma$$

This confirms CPI's ability to match the resolution of quantum interferometry.

3.2 With dispersion

For practical applications, non-linear CPI must be able to retain good resolution with the addition of dispersive materials. As mentioned in section 2.1.5, the dispersive material used in this model was BK7 glass.

Note that a white light interferometer calculation was performed to obtain its resolution as a function of dispersion. The white light values were included in the comparison of CPI methods since they demonstrate the level to which CPI is insensitive to dispersion.

The model code was run for $L = 0$ to $L = 6\ mm$ of BK7 glass, in increments of 0.1 mm. The results are plotted in figure 10. In this plot, the amount of glass, which measures the amount of dispersion, is on the x-axis, and the dip width is on the y-axis.

Figure 10: Comparison of white light (blue), linear CPI (black), and non-linear CPI (red)

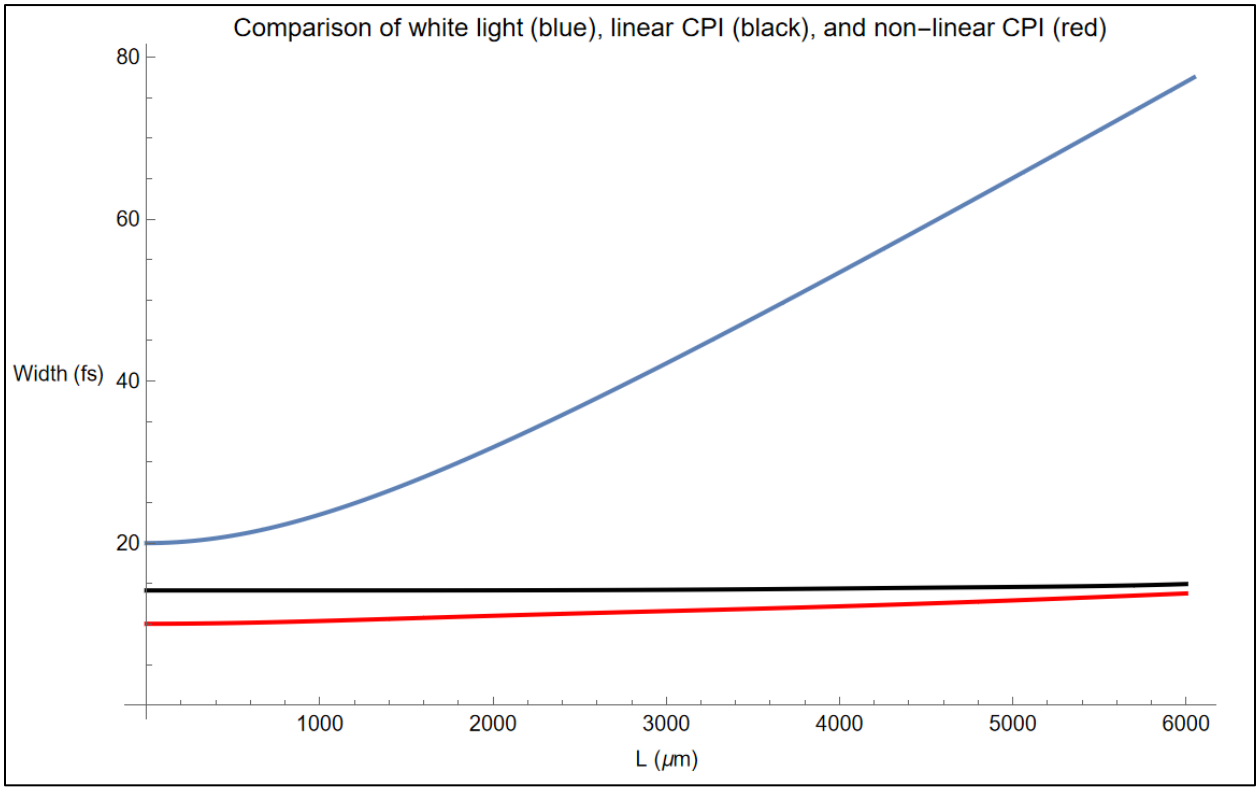

There are a few key remarks to be made about these results. To begin, the white light interferometer's sensitivity to dispersion is quite large compared to both types of CPI. After only introducing 2.8 mm of glass, the width of the signal had doubled, going from 20 fs to 40.3 fs.

$$\Delta\tau_{white\ light} = 40.3\ \text{fs} = 2.01\ (2\sigma)$$

In comparison, the value of the CPI widths, at 2.8 mm of glass, were

$$\Delta\tau_{CPI,linear} = 14.218\ \text{fs} = 1.0054\ (\sqrt{2}\sigma)$$

$$\Delta\tau_{CPI,non-linear} = 11.50\ \text{fs} = 1.15\ (\sigma)$$

For 2.8 mm of glass, the linear CPI width increased by 0.54% and the non-linear CPI width increased by 15%, whereas the white light interferometer method increased by 100%. Therefore, for an amount of dispersion that degraded the white light resolution by a factor of 2, the linear and non-linear CPI resolutions only decreased by a small fraction of their original widths.

Now that the advantage over white light interferometry has been quantified, the behaviour of the two CPI techniques can be examined closely. It can be seen that the increase in dip width is very gradual on this scale, and so figure 11 contains the same dataset as figure 13, but without the white light interferometer results.

Figure 11: Comparison of linear (black) and non-linear (red) CPI

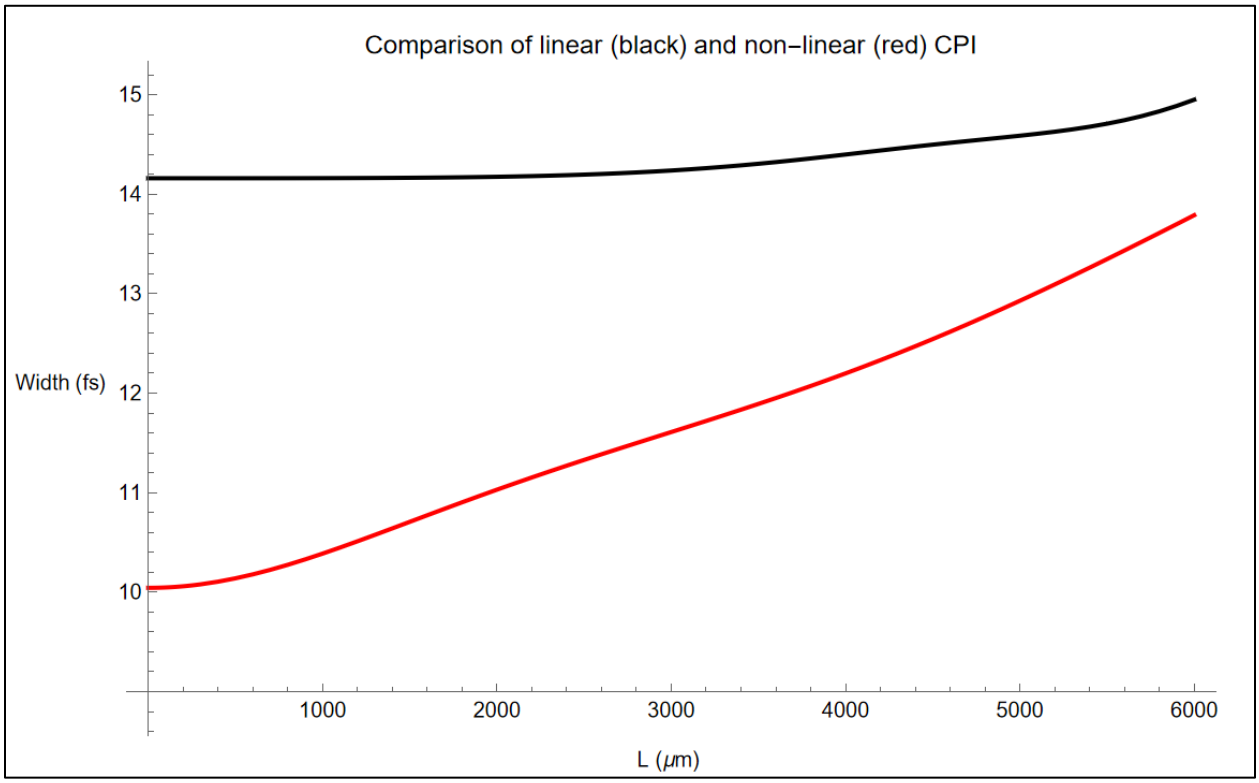

In this plot, the non-linear CPI widths increase faster than the linear version. This implies that there will be some value of L for which the resolution of the non-linear method becomes worse than the linear method. Unfortunately, the difficulty with investigating this limit is that the dip shapes become deformed for large amounts of dispersion, preventing an accurate fit and thus causing a poor measurement of the width. Moreover, the long computation times of each new value of L made it difficult to obtain large data sets within the time constraints of this project. However, it was found that up to 15 mm of BK7 glass, the non-linear CPI technique retained the best resolution.

In summary, for a very large range of dispersive material, the non-linear CPI performs better than the linear CPI, thus making it an improvement in CPI techniques.

Even after putting in 6 mm of dispersive material, the widths only increase to:

$$\Delta\tau_{CPI,linear} = 14.949 \text{ fs } = 1.057\ (\sqrt{2}\sigma)$$

$$\Delta\tau_{CPI,non-linear} = 13.79 \text{ fs } = 1.379\ (\sigma)$$

Therefore, over the entire range of dispersion examined in this research, the linear signal width increases by 5.7%, and the non-linear signal width increases by 37.9%. It is worth noting that the white light result at 6 mm is nearly 4 times worse than the resolution without dispersion. This reinforces the previously proven results that CPI is a classical interferometry technique that exhibits dispersion cancellation. Moreover, this result demonstrates that a significant amount of dispersive material can be added into the non-linear CPI interferometer before the resolution becomes significantly impacted.

3.3 Summary of results

In the following table, the results from this section have been summarized. The widths of the signal from linear and non-linear CPI are presented, along with the HOM and white light interferometer methods.

Table 3: Summary of results, for $\sigma = 10$ fs

Method	Signal width, no dispersion (fs)	Signal width, 6mm of BK7 (fs)
White light interferometer	20.01	77.6
Linear CPI	14.1422	14.949
Non-linear CPI	10.043	13.79
HOM interferometer	10	–

3.4 Super-erf CPI

In section 2.3, it is explained that the non-linear phase function stretches the pulse such that all frequencies contribute equally to the SFG intensity signal. It was shown in the sections above that this non-linear CPI method produces a resolution comparable to that of the analogous quantum system, the HOM interferometer. However, this research went one step further, investigating the possibility of even better resolution.

It follows from the explanation in section 2.3 that having a phase function which stretches the edges of the pulse more than the middle would result in an even narrower signal in time. Instead of a top hat pulse, the goal would be to find $\phi(\omega)$ such that the pulse resembles a shallow bowl, as sketched in figure 12.

Figure 12: Intensity profile for a super-erf chirped pulse

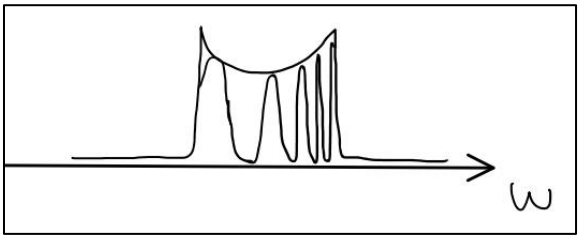

This phase function would be similar to the non-linear chirp, but with more stretching. This is achieved by changing A_{erf}, as well as the coefficient in front of the $(\omega - \omega_0)$ term. This new

method is referred to as “super-erf” since it is a stronger non-linear chirp, still proportional to an error function. Note that this method was investigated without applying dispersion.

One of the challenges of using super-erf is that the intensity signal starts to break down for large amounts of stretching. This can be seen in the dip shapes of the signal. For large non-linear chirp, the “shoulders” of the dip become deformed, and this makes it difficult to fit the shape with a Gaussian function, preventing an accurate measurement of the width. One example of these deformed dip shapes is pictured in figure 13. This was obtained for the following phase function:

$$\phi_{\pm}(\omega) = \pm\mathbf{93}\left[\frac{e^{-x^2}-1}{\sqrt{\pi}} + x\,\mathrm{erf}(x)\right], \qquad x = \frac{\mathbf{3}(\omega-\omega_0)\sigma}{\sqrt{2\log(256)}}$$

In this function, the two parameters that were modified to produce super-erf pulses are highlighted. Note that the original values were **93** and **2** (section 2.3).

Figure 13: Deformed signal dip

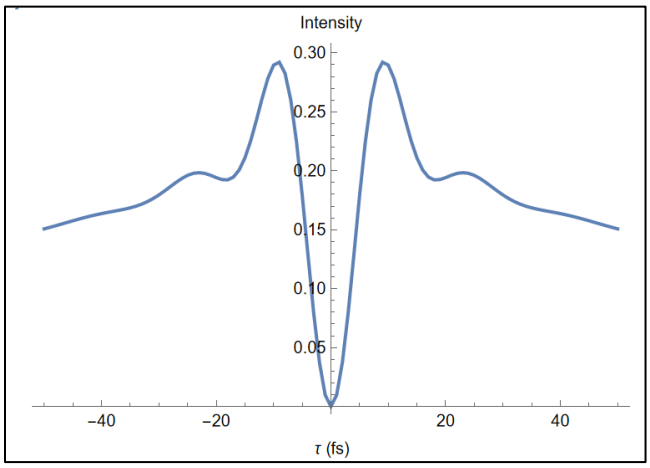

Evidently, fitting the curve in figure 13 might result in a less accurate value for the FWHM. However, by modifying the coefficients in expression for $x(\omega)$, it was possible to find a well-shaped dip that could be reliably fitted. This was achieved with the following phase function:

$$\phi_{\pm}(\omega) = \pm\mathbf{93}\left[\frac{e^{-x^2}-1}{\sqrt{\pi}} + x\,\mathrm{erf}(x)\right], \qquad x = \frac{\mathbf{2.24}(\omega-\omega_0)\sigma}{\sqrt{2\log(256)}}$$

The corresponding super-erf chirped pulse is shown in figure 14, and the dip is presented in figure 15.

Figure 14: Intensity profiles for linear (red) and super-erf (blue) chirped pulses

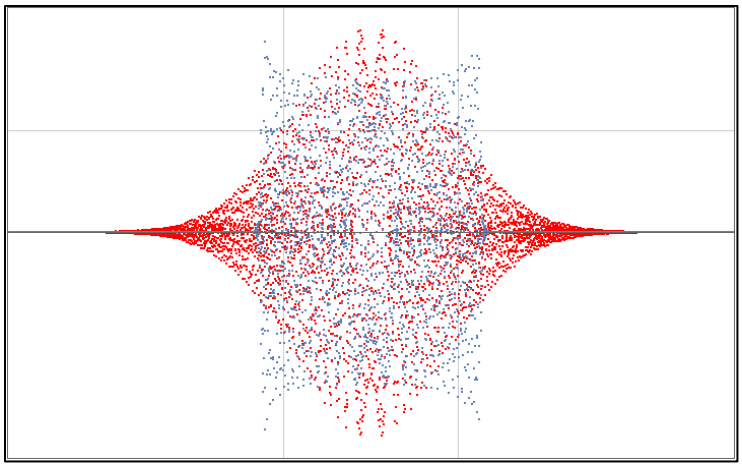

Figure 15: Signal dip for super-erf CPI

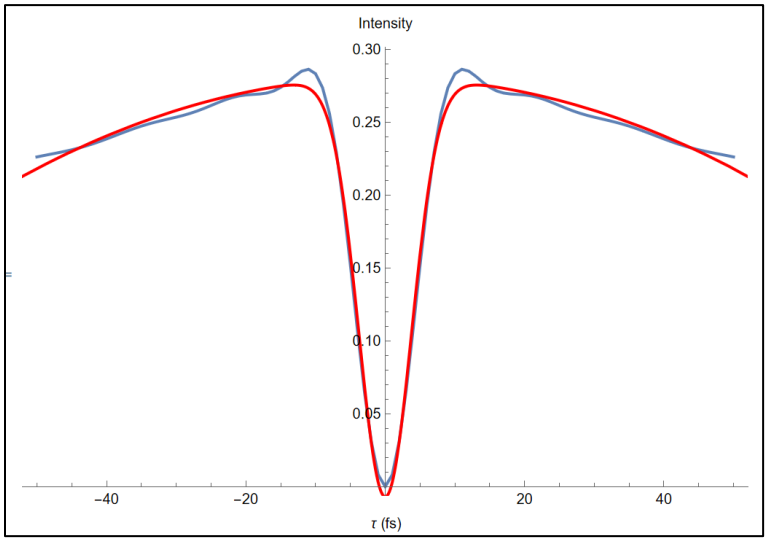

The fitting parameters for this dip gave a FWHM of 8.933 fs, an 11% improvement over the results from non-linear CPI and the HOM system.

$$\Delta\tau_{CPI,super-erf} = 8.933 \text{ fs } = 0.8933\ (\sigma)$$

This proves that it is possible to achieve better resolution using a super-erf phase function to chirp the pulses. Further investigations into the two chirping parameters and their effect on the shape of the dip are required to understand better the extent of this enhancement.

4 Concluding remarks

In summary, it was demonstrated that CPI, a classical interferometry system, can have the same signal resolution as an analogous quantum system. This was achieved using a non-linear phase function to chirp the pulses. Ultimately, this eliminates the last remaining quantum advantage in the field of dispersion-cancelled interferometry.

For an interferometer model with a 10 fs pulse without dispersion, the width of the signal for linear CPI was found to be 14.1422 fs, which agrees with the predicted result. The width of the signal for non-linear CPI was determined to be 10.043 fs, which makes it equal to the resolution of the HOM system.

This non-linear CPI system also exhibited dispersion cancellation for large amounts of dispersive material. The signal width was investigated for a maximum of 6 mm of BK7 glass, which resulted in a 38% increase in the signal width. At all amounts of dispersion investigated in this research, the non-linear CPI performed better than the linear CPI and the white light interferometer.

This is important for applications such as optical coherence tomography, which takes measurements of biological samples. The traditional OCT method uses white light interferometry, which is sensitive to dispersion, as seen in figure 10. Quantum OCT, while theoretically providing better resolution, presents challenges in terms of feasibility and detection abilities. This research demonstrates that the classical chirped pulse interferometry system can achieve the same resolution as QOCT while retaining the advantage of having a high-intensity output.

Further enhancement of non-linear CPI resolution was also considered in this project, known as the “super-erf” method. Despite challenges in obtaining a well-shaped signal for fitting, it was found that super-erf CPI can achieve a width of 8.933 fs, which is approximately a 10% improvement over the resolution of non-linear CPI and HOM interferometers.

As the next steps in this research, it is recommended that the super-erf method be investigated further. By thoroughly examining the effect of the chirping strength coefficients, it might be possible to improve the resolution of the signal even more. Moreover, it is proposed that the feasibility of applying these non-linear chirped pulses in an experimental set-up be evaluated. This would require creating a model which includes constraints for laboratory equipment, such as spatial light modulators, the devices used to chirp pulses.

5 Acknowledgments

This work would not have been possible without the support, expertise, and patience of my supervisor, Kevin Resch. I would like to thank Dr. Resch for always being passionate about this research and for guiding me through each phase of this project.

I would also like to acknowledge the work done by Michael Mazurek, a former MSc student in Dr. Resch’s group. His thesis helped me understand many of the concepts presented in this report, and his work on non-linear chirped pulses was a great foundation to guide my research.

References

[1] Kaltenbaek, R., Lavoie, J., Biggerstaff, D. N., & Resch, K. J. (2008). Quantum-inspired interferometry with chirped laser pulses. *Nature Physics*, 4(11), 864–868. https://doi.org/10.1038/nphys1093

[2] Hariharan, P. (2012). *Basics of interferometry.* Academic Press.

[3] Hong, C. K., Ou, Z. Y., & Mandel, L. (1987). Measurement of subpicosecond time intervals between two photons by interference. *Physical Review Letters*, 59(18), 2044–2046. https://doi.org/10.1103/physrevlett.59.2044

[4] Hecht, E. (2002). Optics.

[5] Steinberg, A. M., Kwiat, P. G., & Chiao, R. Y. (1992). Dispersion cancellation in a measurement of the single-photon propagation velocity in glass. *Physical Review Letters*, 68(16), 2421–2424. https://doi.org/10.1103/physrevlett.68.2421

[6] Kaltenbaek, R., Lavoie, J., & Resch, K. J. (2009b). Classical analogues of Two-Photon quantum interference. *Physical Review Letters*, 102(24). https://doi.org/10.1103/physrevlett.102.243601

[7] Popescu, D. P., Choo-Smith, L., Flueraru, C., Mao, Y., Chang, S., Disano, J., Sherif, S., & Sowa, M. G. (2011). Optical coherence tomography: fundamental principles, instrumental designs and biomedical applications. *Biophysical Reviews*, 3(3), 155–169. https://doi.org/10.1007/s12551-011-0054-7

[8] Abouraddy, A. F., Nasr, M. B., Saleh, B. E. A., Sergienko, A. V., & Teich, M. C. (2002). Quantum-optical coherence tomography with dispersion cancellation. *Physical Review A*, 65(5). https://doi.org/10.1103/physreva.65.053817

[9] Nasr, M. B., Goode, D. P., Nguyen, N., Rong, G., Yang, L., Reinhard, B. M., Saleh, B. E., & Teich, M. C. (2008). Quantum optical coherence tomography of a biological sample. *Optics Communications*, 282(6), 1154–1159. https://doi.org/10.1016/j.optcom.2008.11.061

[10] Nasr, M. B., Saleh, B. E. A., Sergienko, A. V., & Teich, M. C. (2003). Demonstration of Dispersion-Canceled Quantum-Optical Coherence tomography. *Physical Review Letters*, 91(8). https://doi.org/10.1103/physrevlett.91.083601

[11] Altepeter, J. B., Jeffrey, E. R., & Kwiat, P. G. (2005). Phase-compensated ultra-bright source of entangled photons. *Optics Express,* 13(22), 8951. https://doi.org/10.1364/opex.13.008951

[12] Boyd, R. W. (2008). *Nonlinear optics*. Elsevier.

[13] Paschotta, R. (2024, October 18). Sellmeier formula. 2024 RP Photonics AG. https://www.rp-photonics.com/sellmeier_formula.html#ref1

[14] Coadou, E. (2018). Propagation, Dispersion and Measurement of sub-10 fs Pulses. In www.coherent.com. Coherent. https://www.coherent.com/resources/tech-notes/lasers/PropagationDispersionMeasurement_of_sub_10fsPulses_08_29_18.pdf

[15] Mazurek, M. (2013). Dispersion-cancelled imaging with chirped laser pulses. https://dspacemainprd01.lib.uwaterloo.ca/server/api/core/bitstreams/34ac8b59-3f72-4e30-967f-b80f6e5087b4/content